Determination of *s-d* exchange coupling in GaMnN by time-resolved Kerr rotation spectroscopy

Wei-Ting Hsu,[1] Ting-Yen Hsieh,[1] Hsin-Feng Chen,[1] Feng-Wen Huang,[2] Po-Cheng Chen,[2]
Jinn-Kong Sheu,[2] and Wen-Hao Chang[1,*]

[1]*Department of Electrophysics, National Chiao Tung University, Hsinchu 30010, Taiwan*
[2]*Department of Photonics, National Cheng Kung University, Tainan 70101, Taiwan*

(Received 9 September 2013; revised manuscript received 25 August 2014; published 29 September 2014)

Coherent electron-spin dynamics in $Ga_{1-x}Mn_xN$ has been investigated by time-resolved Kerr rotation spectroscopy. The effective electron g factor shows a linear increase with the Mn concentration due to the *s-d* exchange coupling between the conduction electrons and the *d*-shell electrons of Mn^{3+} impurities. The magnitude and sign of the *s-d* exchange constant are determined precisely to be $N_0\alpha = +0.23 \pm 0.02$ eV, indicative of a ferromagnetic *s-d* exchange coupling in GaMnN. The determined $N_0\alpha$ is consistent with the typical value found in most diluted magnetic semiconductors and reveals that GaMnN is indeed not an exception.

DOI: 10.1103/PhysRevB.90.125205 PACS number(s): 78.55.Qr, 78.20.Ls, 78.55.Cr, 78.67.Lt

I. INTRODUCTION

Wide band-gap diluted magnetic semiconductors (DMSs) [1], such as GaN and ZnO doped with transition metals, have been an interesting class of magnetic materials since the prediction of ferromagnetism above room temperature [2,3]. Apart from their potential applications in semiconductor spintronics, GaN-based III-V DMSs are particularly attractive for the development of spin-based optoelectronics due to their compatibility with the mature technology of solid-state lighting. To realize various spin-based device functionalities, it is essential to have a deeper understanding of the *s-d* (*p-d*) exchange coupling, characterized by the exchange constant $N_0\alpha$ ($N_0\beta$), between the *s*-like conduction electrons (*p*-like valence holes) and the *d*-shell electrons localized on magnetic dopants.

Magneto-optical (MO) measurements of band-edge excitonic giant Zeeman splitting have long been used to determine the *sp-d* exchange constants in typical II-VI DMSs such as CdMnTe [4]. For GaN [5–7] and ZnO [8,9] based wide band-gap DMSs, however, only *apparent* values of $N_0\alpha$ and $N_0\beta$ can be determined by MO measurements. The magnitudes and signs of the *apparent* $N_0\alpha$ and $N_0\beta$ are ambiguous compared to those determined by x-ray photoemission spectroscopy [10] and by electron paramagnetic resonance (EPR) [11].

The peculiarity of apparent *sp-d* exchange constants determined by MO measurements for GaN [5–7] and ZnO [8,9] based DMSs has been discussed experimentally and theoretically. The strong *p-d* hybridization specific to wide band-gap DMSs [12] can lead to significant renormalization of the valence-band exchange splitting, making the apparent *p-d* exchange constant $N_0\beta$ abnormally small and of opposite sign, which deviates remarkably from the chemical trend predicted by the virtual crystal and mean-field approximations. Furthermore, the sizable electron-hole (*s-p*) exchange interaction between the conduction-band electrons and holes tightly bound to magnetic ions [13] is expected to play a role in the apparent *s-d* exchange constants.

Apart from the peculiarity of apparent exchange constants, it is not straightforward to determine $N_0\alpha$ and $N_0\beta$ separately by MO measurements. Typically only $N_0(\alpha - \beta)$ is accessible by measurements of exciton energy. The reported estimation of $N_0\beta$ is usually obtained by an assumed value of $N_0\alpha$ based on typical II-VI DMSs [4]. In zinc-blend DMSs, such as CdMnTe, $N_0\alpha$ and $N_0\beta$ can be determined separately when the giant Zeeman splittings of both the heavy-hole and light-hole exciton transitions are accessible from MO measurements [4,14]. Similarly, for the wurtzite structure, separate determination of $N_0\alpha$ and $N_0\beta$ is possible when the giant Zeeman splittings of all the free excitons *A*, *B,* and *C* are resolved [7]. However, since the observation of the *C* exciton peak is hindered by the optical selection rule in the Faraday configuration, only the value of $N_0(\alpha - \beta)$ can be determined reliably by MO measurements [5,6,8,9]. Recently, separate determination of both $N_0\alpha$ and $N_0\beta$ of wurtzite GaMnN has been achieved by Suffczyński *et al.* [7] using MO measurements, but with a quite large uncertainty probably due to the relatively weaker signal for the *C* excitons. Nevertheless, the determined apparent $N_0\alpha$ in GaMnN is surprisingly small, which was attributed to a mutual cancellation between the *s-d* and the *s-p* exchange couplings. To date, the value and sign of $N_0\alpha$ in GaMnN remain ambiguous.

In this context, measurement of coherent spin dynamics in DMSs by time-resolved Kerr rotation (TRKR) spectroscopy appears to be an ideal alternative for independent measurements of $N_0\alpha$. Since the hole spin lifetime is much shorter than the electron-spin lifetime, TRKR can selectively probe only the coherent electron-spin precession, which could be inherently free from electron-hole exchange and hence ideal for determining the *s-d* exchange constant (rather than an apparent value) in DMSs. This time-resolved measurement scheme has also been employed to determine $N_0\alpha$ in GaMnAs [15–17] and ZnCoO [18].

Here we report on measurements of coherent electron-spin dynamics in GaMnN by TRKR spectroscopy. The effective electron g factor shows a linear increase with the Mn concentration due to the *s-d* exchange coupling between the conduction electrons and the Mn spins. Photoluminescence (PL) and reflectivity measurements combined with concentration calibration by secondary ion mass spectroscopy (SIMS) reveal that the Mn dopants are mostly incorporated as neutral Mn^{3+} centers with the d^4 configuration. The magnitude and sign of the *s-d* exchange constant are determined independently to

*whchang@mail.nctu.edu.tw

be $N_0\alpha = +0.23 \pm 0.02$ eV, indicative of a ferromagnetic *s-d* exchange coupling in GaMnN.

II. EXPERIMENTS

The samples were grown on *c*-face sapphire substrates by metal-organic vapor-phase epitaxy. The layer structure consists of a 600-nm-thick Mn-doped GaN layer grown on a 2-μm-thick undoped GaN buffer layer. Bismethylcyclopentadienyl manganese [$(MeCp)_2Mn$] was used as the Mn precursor. The growth temperature and pressure for the Mn-doped GaN were 1010 °C and 100 Torr, respectively. Four samples with different Mn precursor flow rates of 0, 100, 300, and 500 SCCM (SCCM denotes cubic centimeter per minute at STP) have been grown, corresponding to Mn concentrations $x = 0$, 0.053, 0.16, and 0.27% as determined by SIMS. PL measurements were carried out at $T = 13$ K using the 325-nm line of a He-Cd laser as an excitation source. The PL signals were analyzed by a 0.75-m monochromator and detected by a liquid-nitrogen-cooled CCD camera. Reflectivity spectra were measured by the same apparatus, except that the light source was replaced by a tungsten-halogen lamp. For TRKR measurements, both pump and probe pulses are produced from the frequency-doubled output of a mode-lock Ti-sapphire laser with pulse width ~150 fs and repetition rate 80 MHz. The wavelength is tuned to the absorption edge of GaN, which is typical in the range of 356–362 nm, depending on temperature. Spin-polarized carriers in GaMnN were excited by a circularly polarized pump pulse. A transverse magnetic field is applied in the Voigt geometry by an electromagnet to induce spin precessions. A linearly polarized probe pulse with a time delay was used to detect the projection of net spin magnetization along the surface normal. The Kerr rotation angle of the reflected probe pulse is analyzed by a polarization bridge using the balanced detection scheme. The circular polarization of the pump beam is modulated with a photoelastic modulator at 50 kHz for lock-in detection.

III. RESULTS AND DISCUSSION

The $Ga_{1-x}Mn_xN$ samples were first examined by PL and reflectivity measurements. Figure 1(a) shows the PL spectra measured at $T = 13$ K for the investigated samples. Emission peaks originated from donor-bound excitons (DBXs) and free excitons A (FX_As) in wurtzite GaN can be resolved in all samples. For Mn-doped GaN, the DBX peak remains fixed at 3.483 eV, but with a relatively weaker intensity than the FX_A peak. In contrast, all the free exciton peaks blueshift systematically with the increasing Mn concentration. As has been discussed in detail in Ref. [7], the blueshift in the free exciton energy can be attributed to the band-gap shift caused by the *p-d* hybridization between the valance band and the Mn impurity states. The unshifted DBX arose from the fact that photocarriers are also generated in the undoped GaN buffer layer. The residual donors in the top $Ga_{1-x}Mn_xN$ layer are compensated by the Mn dopants, leading to a relatively weaker DBX intensity for the Mn doped samples.

The charge state of Mn impurities can be further examined by the intraion optical absorption at 1.41 eV for Mn^{3+} in GaN. Figure 1(c) shows the optical reflectivity spectrum for the $Ga_{1-x}Mn_xN$ sample with $x = 0.27\%$. A clear absorption feature at 1.41 eV superimposed on an interference pattern can be resolved. This absorption dip arises from the internal transition between $^5T_2$ and ^5E levels, which is a characteristic feature specific to Mn^{3+} ions [19–21]. By modeling the Mn^{3+} absorption as a Lorentzian oscillator and considering multilayer interference, an absorption coefficient of $\alpha \approx 8000 \pm 400$ cm^{-1} at the dip was estimated, corresponding to an integrated absorption cross section of 1.65×10^{-23} m^2 eV/Mn, which is in good agreement with the value reported in literature [20]. This leads us to conclude that the Mn impurities are mostly incorporated as neutral centers, i.e., Mn^{3+} charge states with the d^4 configuration. Indeed, since the undoped GaN is weakly *n* type with a residual donor concentration typically less than 10^{17} cm^{-3}, Mn^{2+} is expected to be a minority for Mn doping up to 2–12 $\times 10^{19}$ cm^{-3} investigated here.

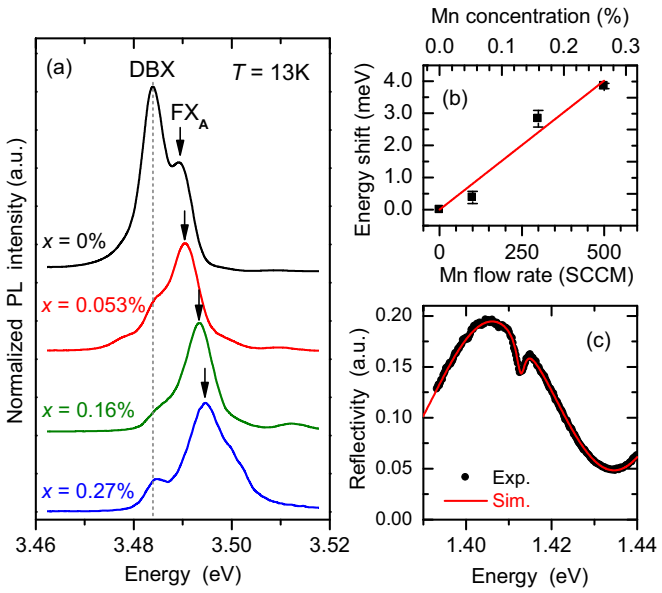

FIG. 1. (Color online) (a) PL spectra measured at $T = 13$ K. The PL intensities have been normalized with respect to the FX_A peak. (b) The energy shift of FX_A as a function of Mn concentration. (c) The reflectivity spectrum for the $x = 0.27\%$ sample.

Figure 2(a) shows the TRKR traces measured at $T = 15$ K in a transverse magnetic field of $B = 0.58$ T for samples with different Mn concentrations. The Kerr rotation angles $\theta_K(t)$ can be described by an exponentially damped oscillatory function: $\theta_K(t) = A\exp(-t/T_2^*)\cos(\omega_L t)$, where T_2^* is the spin lifetime, or alternatively the transverse dephasing time of the spin ensemble, and $\omega_L = g^*\mu_B B/\hbar$ is the Larmor frequency, where g^* is the effective *g* factor and μ_B is the Bohr magneton. Fitting the TRKR trace for the undoped GaN yields a *g* factor of $g^* = 1.95$, consistent with the electron *g* factor in GaN reported in literature [22,23]. Since the hole spin lifetime is much shorter, only the coherent electron-spin dynamics is selectively probed by the TRKR measurements [24]. For Mn-doped GaN, the TRKR traces show an increase in Larmor frequency ω_L and a rapid decrease in spin lifetime T_2^*, as shown in Figs. 2(b) and 2(c). The variation of spin lifetime on the Mn concentration can be attributed to the local magnetization fluctuations of the Mn impurities [18,25]. We found that the

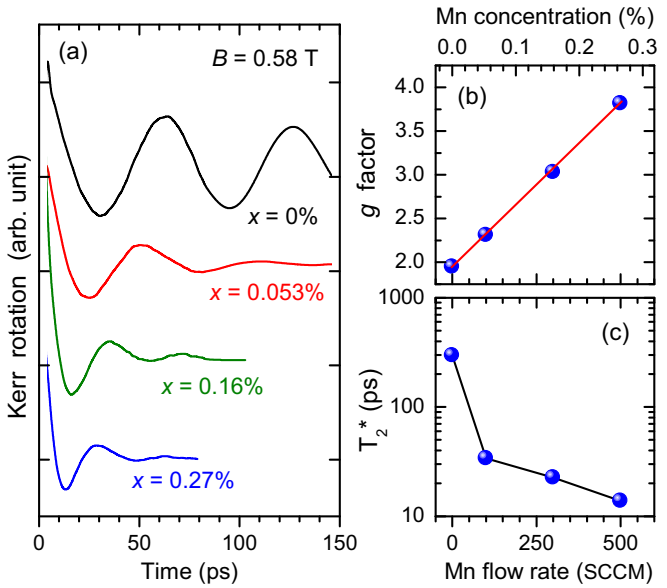

FIG. 2. (Color online) (a) TRKR spectra measured at $T = 15$ K and $B = 0.58$ T. (b) The deduced effective g factor and (c) the spin lifetime T_2^* as a function of Mn concentration.

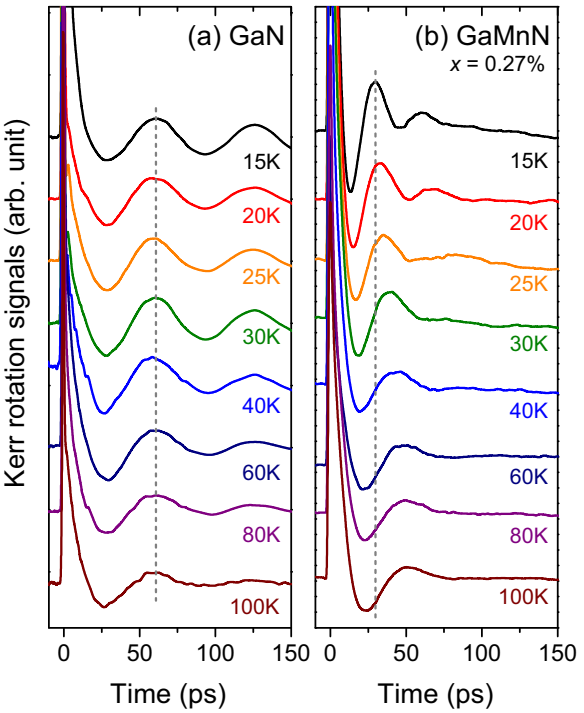

FIG. 3. (Color online) Temperature-dependent TRKR spectra taken at $B = 0.58$ T for (a) the undoped GaN and (b) the $Ga_{1-x}Mn_xN$ with $x = 0.27\%$ samples.

deduced T_2^* varies approximately as $\sim 1/x$, in agreement with the model considering local magnetization fluctuations for low Mn concentrations [25].

In Fig. 2(b), the linear increase in the electron g factor g^* with the Mn concentration x is a direct consequence of exchange coupling between the electrons and the Mn impurities in DMS [24]. The magnetic field induced splitting is affected not only by the Zeeman effect but also by the electron-Mn^{3+} s-d exchange coupling. The effective electron g factor g^* in the virtual crystal and mean field approximations is given by [4,26]

$$g^* = g_0 - \frac{x N_0 \alpha \langle S_x \rangle}{\mu_B B}, \tag{1}$$

where $g_0 = 1.95$ is the electron g factor in GaN without magnetic dopants, $N_0\alpha$ is the s-d exchange coupling constant, and $\langle S_x \rangle$ is the mean spin of Mn^{3+} ions along the transverse magnetic field. The mean spin $\langle S_x \rangle$ can be described by Brillouin function $B_S(T, B)$ according to the equilibrium populations of the four electron-spin states of a Mn^{3+} impurity with a total spin of $S = 2$ as a function of magnetic field B and temperature T. Since the mean spin $\langle S_x \rangle$ by convention is negative, the linear increase in g^* with x shown in Fig. 2(b) implies that the s-d exchange coupling constant $N_0\alpha$ is positive, i.e., the electron-Mn^{3+} interaction is ferromagnetic.

The influence of s-d exchange on the effective electron g factor can be further examined by temperature-dependent measurements. Since the Mn mean spin $\langle S_x \rangle$ depolarizes with the increasing temperature in accordance with the Brillouin function, the effective g factor g^* is also expected to decrease with temperature in the same manner. Figures 3(a) and 3(b) show the temperature evolutions of TRKR traces for the $x = 0$ and 0.27% samples at $B = 0.58$ T. For the undoped GaN, the oscillation periods are essentially the same for all temperatures, indicative of a temperature-independent electron g factor. In contrast, an increasing oscillation period is observed for the $x = 0.27\%$ sample. The deduced effective g factor shows a rapidly decreasing g^* for $T < 100$ K and approaching $g^* = 1.95$ at higher temperatures.

Figure 4 summarizes the measured effective g factor g^* as a function of Mn concentration and temperature. The error bars in determining the g factor are also included in Fig. 4(a). By fitting the linear dependence of g^* on x and the temperature-dependent g^* to Eq. (1) with $S = 2$, we determine the s-d exchange constant to be $N_0\alpha = 0.23 \pm 0.02$ eV, which is in very good agreement with the typical value in the range of $N_0\alpha \sim 0.2$–0.25 eV for most DMSs [4,26]. This means that GaMnN is indeed not an exception. We noted that the determined $N_0\alpha$ is large in comparison with $N_0\alpha = +14$ meV determined by EPR [11] and $N_0\alpha = 0.0 \pm 0.1$ eV determined by MO measurements [7]. Since the EPR measurements by

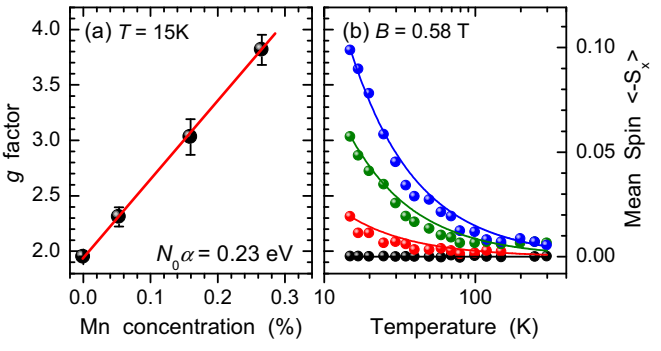

FIG. 4. (Color online) The evolution of the effective electron g factor with (a) the Mn concentration and (b) the temperature.

Wolos *et al.* [11] were conducted in *n*-type GaMnN ($n \sim 10^{19}$ cm^{-3}), where the majority of Mn dopants are in the Mn^{2+} charge state, the apparent $N_0\alpha$ is reduced remarkably by the Coulomb repulsive potential of the negatively charged Mn^{2+} centers [13] and the electrostatic screening caused by the high-density conduction electrons. For the MO measurements by Suffczyński *et al.* [7], where the investigated GaMnN have high resistivity and predominant Mn^{3+}, the measured small apparent $N_0\alpha$ was attributed to a mutual compensation by a sizable *s-p* exchange coupling between conduction electrons and holes bound to Mn impurities (i.e., the $d^5 + h$ configuration) [13]. In our case, the electrostatic repulsion and screening can be excluded in the high-resistivity GaMnN with a majority of Mn^{3+}. The larger and positive $N_0\alpha$ value revealed here implies that the influence of the electron-hole *s-p* exchange coupling is insignificant in our measurements. Here we argue that the time-resolved measurements of coherent electron-spin dynamics are inherently free from the electron-hole exchange coupling due to the rapid hole spin dephasing time. In TRKR measurements, spin-polarized electrons and holes (s_z and J_z) are created by a circularly polarized pump pulse. Both the electron and hole spins are expected to precess about the applied transverse magnetic field ($\vec{B} \| \hat{x}$) but with different Larmor frequencies determined by their effective *g* factors. However, due to the much shorter hole spin dephasing time, the hole spin precession is not resolved in the TRKR traces. The electron-hole exchange interactions thus occur between the long-lived electron spins and the depolarized hole spins, leading to a net zero *s-p* exchange splitting. This is different from the case in MO measurements, where both the electrons and holes are subjected to a longitudinal field ($\vec{B} \| \hat{z}$); the electron-hole *s-p* exchange coupling thus contributes to the total spin splitting and hence alters the determination of the *s-d* exchange constant.

Before concluding, we would like to point out that the time-resolved measurements presented here cannot distinguish whether the conduction electrons are interacting with the neutral Mn^{3+} centers (d^4) or with the complex formed by Mn^{2+} plus a bound hole ($d^5 + h$). Although a majority of Mn^{3+} has been confirmed by reflectivity measurements for our samples, a fraction of the d^4 configuration could be photoionized to the $d^5 + h$ complex under optical excitations by the pump pulses during TRKR measurements. Experimental evidence for the photoionization of Mn^{3+} has been reported by photoconductivity [27] and photoassisted EPR [28] measurements. The presence of ionized Mn^{2+} centers would alter the $N_0\alpha$ value somewhat, since the mean spin $\langle S_x \rangle$ in Eq. (1) should be replaced by a mixture of $S = 5/2$ and 2. According to the excitation power used in our experiments, we estimate that the photogenerated carriers ($\lesssim 10^{18}$ cm^{-3}) are unable to create a significant amount of Mn^{2+} in our samples with Mn doping levels up to (2–12) $\times 10^{19}$ cm^{-3}. At most only less than 5% of the Mn^{3+} would be photoionized to Mn^{2+}, corresponding to an insignificant correction to the $N_0\alpha$ value by less than 5 meV.

IV. CONCLUSION

In summary, the coherent electron-spin dynamics in $Ga_{1-x}Mn_xN$ with $x \lesssim 0.27\%$ has been investigated by TRKR measurements. The effective electron *g* factor shows a linear increase with the Mn concentration due to the *s-d* exchange coupling between the conduction electrons and the localized Mn spins. PL and reflectivity measurements combined with concentration calibration by SIMS confirmed that the majority of Mn dopants are in the Mn^{3+} charge state with the d^4 configuration. The magnitude and sign of the *s-d* exchange constant are determined independently to be $N_0\alpha = +0.23 \pm 0.02$ meV, indicative of a ferromagnetic electron-Mn^{3+} interaction in Mn-doped GaN. This value is in very good agreement with the typical *s-d* exchange constant found in most DMSs and reveals that GaMnN is indeed not an exception. We pointed out that the time-resolved measurements of coherent electron-spin dynamics are inherently free from the electron hole exchange coupling and can be a promising method for determining the *s-d* exchange constant in wide band-gap DMSs.

ACKNOWLEDGMENTS

This work was supported in part by the Ministry of Education Aiming for the Top University (MOE-ATU) program and the Ministry of Science and Technology of Taiwan under Grants No. NSC-101-2628-M-009-002-MY3 and No. NSC 103-2923-M-009-002-MY3. W.H.C. acknowledges support from the Center for Interdisciplinary Science under the MOE-ATU program for National Chiao Tung University.

[1] C. Liu, F. Yun, and H. Morkoç, J. Mater. Sci.: Mater. Electron. **16**, 555 (2005).
[2] T. Dietl, H. Ohno, F. Matsukura, J. Cibert, and D. Ferrand, Science **287**, 1019 (2000).
[3] T. Dietl, H. Ohno, and F. Matsukura, Phys. Rev. B **63**, 195205 (2001).
[4] J. Kossut and J. A. Gaj, *Introduction to the Physics of Diluted Magnetic Semiconductors* (Springer, New York, 2010).
[5] W. Pacuski, D. Ferrand, J. Cibert, J. A. Gaj, A. Golnik, P. Kossacki, S. Marcet, E. Sarigiannidou, and H. Mariette, Phys. Rev. B **76**, 165304 (2007).
[6] W. Pacuski, P. Kossacki, D. Ferrand, A. Golnik, J. Cibert, M. Wegscheider, A. Navarro-Quezada, A. Bonanni, M. Kiecana, M. Sawicki, and T. Dietl, Phys. Rev. Lett. **100**, 037204 (2008).
[7] J. Suffczyński, A. Grois, W. Pacuski, A. Golnik, J. A. Gaj, A. Navarro-Quezada, B. Faina, T. Devillers, and A. Bonanni, Phys. Rev. B **83**, 094421 (2011).
[8] W. Pacuski, D. Ferrand, J. Cibert, C. Deparis, J. A. Gaj, P. Kossacki, and C. Morhain, Phys. Rev. B **73**, 035214 (2006).
[9] W. Pacuski, J. Suffczyński, P. Osewski, P. Kossacki, A. Golnik, J. A. Gaj, C. Deparis, C. Morhain, E. Chikoidze, Y. Dumont, D. Ferrand, J. Cibert, and T. Dietl, Phys. Rev. B **84**, 035214 (2011).
[10] J. I. Hwang, Y. Ishida, M. Kobayashi, H. Hirata, K. Takubo, T. Mizokawa, A. Fujimori, J. Okamoto, K. Mamiya, Y. Saito *et al.*, Phys. Rev. B **72**, 085216 (2005).
[11] A. Wolos, M. Palczewska, Z. Wilamowski, M. Kaminska, A. Twardowski, M. Bockowski, I. Grzegory, and S. Porowski, Appl. Phys. Lett. **83**, 5428 (2003).

[12] T. Dietl, Phys. Rev. B **77**, 085208 (2008).
[13] C. Śliwa and T. Dietl, Phys. Rev. B **78**, 165205 (2008).
[14] J. A. Gaj, R. Planel, and G. Fishman, Sol. State Commun. **29**, 435 (1979).
[15] R. C. Myers, M. Poggio, N. P. Stern, A. C. Gossard, and D. D. Awschalom, Phys. Rev. Lett. **95**, 017204 (2005).
[16] M. Poggio, R. C. Myers, N. P. Stern, A. C. Gossard, and D. D. Awschalom, Phys. Rev. B **72**, 235313 (2005).
[17] N. P. Stern, R. C. Myers, M. Poggio, A. C. Gossard, and D. D. Awschalom, Phys. Rev. B **75**, 045329 (2007).
[18] K. M. Whitaker, M. Raskin, G. Kiliani, K. Beha, S. T. Ochsenbein, N. Janssen, M. Fonin, U. Rüdiger, A. Leitenstorfer, D. R. Gamelin, and R. Bratschitsch, Nano Lett. **11**, 3355 (2011).
[19] A. Wolos, A. Wysmolek, M. Kaminska, A. Twardowski, M. Bockowski, I. Grzegory, S. Porowski, and M. Potemski, Phys. Rev. B **70**, 245202 (2004).
[20] S. Marcet, D. Ferrand, D. Halley, S. Kuroda, H. Mariette, E. Gheeraert, F. J. Teran, M. L. Sadowski, R. M. Galera, and J. Cibert, Phys. Rev. B **74**, 125201 (2006).
[21] A. Bonanni, M. Sawicki, T. Devillers, W. Stefanowicz, B. Faina, T. Li, T. E. Winkler, D. Sztenkiel, A. Navarro-Quezada, M. Rovezzi, R. Jakieła, A. Grois, M. Wegscheider, W. Jantsch, J. Suffczyński, F. D'Acapito, A. Meingast, G. Kothleitner, and T. Dietl, Phys. Rev. B **84**, 035206 (2011).
[22] B. Beschoten, E. Johnston-Halperin, D. K. Young, M. Poggio, J. E. Grimaldi, S. Keller, S. P. DenBaars, U. K. Mishra, E. L. Hu, and D. D. Awschalom, Phys. Rev. B **63**, 121202(R) (2001).
[23] C. Y. Hu, K. Morita, H. Sanada, S. Matsuzaka, Y. Ohno, and H. Ohno, Phys. Rev. B **72**, 121203(R) (2005).
[24] S. A. Crooker, D. D. Awschalom, J. J. Baumberg, F. Flack, and N. Samarth, Phys. Rev. B **56**, 7574 (1997).
[25] K. E. Rönnburg, E. Mohler, H. G. Roskos, K. Ortner, C. R. Becker, and L. W. Molenkamp, Phys. Rev. Lett. **96**, 117203 (2006).
[26] J. K. Furdyna, J. Appl. Phys. **64**, R29 (1988).
[27] T. Graf, S. T. B. Goennenwein, and M. S. Brandt, Phys. Status Solidi B **239**, 277 (2003).
[28] A. Wolos, M. Palczewska, M. Zajac, J. Gosk, M. Kaminska, A. Twardowski, M. Bockowski, I. Grzegory, and S. Porowski, Phys. Rev. B **69**, 115210 (2004).